Infrared Colloidal Quantum Dot Image Sensors

Vladimir Pejović, Epimitheas Georgitzikis, Jiwon Lee, Itai Lieberman, David Cheyns, Paul Heremans, and Paweł E. Malinowski, *Member, IEEE*

(Invited Paper)

***Abstract*— Quantum dots (QDs) have been explored for many photonic applications, both as emitters and absorbers. Thanks to the bandgap tunability and ease of processing, they are prominent candidates to disrupt the field of imaging. This review article illustrates the state of technology for infrared image sensors based on colloidal QD absorbers. Up to now, this wavelength range has been dominated by III–V and II–VI imagers realized using flip-chip bonding. Monolithic integration of QDs with the readout chip promises to make short-wave infrared (SWIR) imaging accessible to applications that could previously not even consider this modality. Furthermore, QD sensors show already state-of-the-art figures of merit, such as sub-2-μm pixel pitch and multimegapixel resolution. External quantum efficiencies already exceed 60% at 1400 nm. With the potential to increase the spectrum into extended SWIR and even mid-wave infrared, QD imagers are a very interesting and dynamic technology segment.**

***Index Terms*— Colloidal quantum dot (CQD) image sensors, infrared imaging, lead sulfide (PbS), mercury telluride (HgTe), short-wave infrared (SWIR) image sensors.**

I. Introduction

SHORT-WAVE infrared (SWIR) spectrum has been explored for decades for low-light imaging and detection of "invisible" light sources. With the introduction of in-bump hybrid bonding in the mid-1970s, focal plane arrays (FPAs) based on compound semiconductors such as InGaAs and HgCdTe enabled photograph and video acquisition in the SWIR range [1]. The early developments were centered around military and defense applications, for better detecting camouflaged people and objects as well as laser sources. Other applications followed, with cameras for scientific, space and industrial uses as the most prominent fields. Up to now, the deployment of SWIR cameras has been limited to such high-end niches due to very high prices of systems for this range, typically in excess of several 1000 USD/unit. Some models are advertised as "affordable," but the resolution is then typically limited to 320 × 256 pixels [2], [3]. High-temperature epitaxy (typically on small wafers—3 in/4 in) and hybridization (typically die-to-die) make for low throughput (lab rather than fab manufacturing) and thus high cost. In addition, pixel pitch is limited by the in-bump and hybridization process, with commercial sensors rarely going below 15 μm. A common FPA resolution is still video graphic array (VGA), with some extended graphic array (XGA) sensors appearing [4]–[9]. The most recent 5-μm pitch sensors hybridized by Cu–Cu bonding are a breakthrough [10]. Nevertheless, they are almost an order of magnitude away from the state-of-the-art complementary metal-oxide-semiconductor (CMOS) image sensors (CISs), and are still based on InGaAs, with all the limitations thereof. A common pixel architecture used in such imagers is also quite complex, based on the capacitive transimpedance amplifier (CTIA) [11]. It is feasible with the footprint available in the large pixel pitch but also necessary for good control of a low bias voltage on the photodiode. Its disadvantage is higher static power consumption during signal integration.

Image sensors based on a monolithic approach, with a pixel stack processed directly on the CMOS readout, have been attracting attention as a much simpler integration approach. If a sufficiently efficient infrared absorber can be integrated as a part of the back-end-of-line foundry process, there are no hybrid limitations: pixel pitch is defined by the readout, resolution can be maximized (and extended with stitching) and throughput increased, resulting in a scalable and truly affordable solution. Thin-film absorbers such as organic semiconductors, hybrid perovskites, or colloidal quantum dots (QDs) are proposed as one of the routes to realize high pixel density and high-resolution FPAs [12], [13], enabling new imaging applications requiring multimillion units, such as machine vision, consumer, and automotive.

In this review article, we give an overview of the infrared imaging technology based on thin-film photodetectors using QDs as an absorber and realized through a "monolithic hybrid" integration approach. The following section gives a historical perspective and mentions some of the key milestones. Then, the most important academic groups and companies active in the field are covered, and pros and cons of each approach are discussed. Majority of the content discusses image sensors for the SWIR range (1.4–2.5 μm), as the main target for most of the examples found in the literature and on the market, but examples of image sensors working in the near infrared (NIR)

Manuscript received September 30, 2021; revised November 19, 2021; accepted November 19, 2021. Date of publication December 20, 2021; date of current version May 24, 2022. The review of this article was arranged by Editor R. M. Guidash. *(Corresponding author: Paweł E. Malinowski.)*

Vladimir Pejović and Paul Heremans are with IMEC, 3001 Leuven, Belgium, and also with the Department of Electrical Engineering (ESAT), KU Leuven, 3001 Leuven, Belgium.

Epimitheas Georgitzikis, Jiwon Lee, Itai Lieberman, David Cheyns, and Paweł E. Malinowski are with IMEC, 3001 Leuven, Belgium (e-mail: pawel.malinowski@imec.be).

Color versions of one or more figures in this article are available at https://doi.org/10.1109/TED.2021.3133191.

Digital Object Identifier 10.1109/TED.2021.3133191

0018-9383 © 2021 IEEE. Personal use is permitted, but republication/redistribution requires IEEE permission.
See https://www.ieee.org/publications/rights/index.html for more information.

Authorized licensed use limited to: Biruni Universitesi. Downloaded on November 13,2022 at 13:03:58 UTC from IEEE Xplore. Restrictions apply.

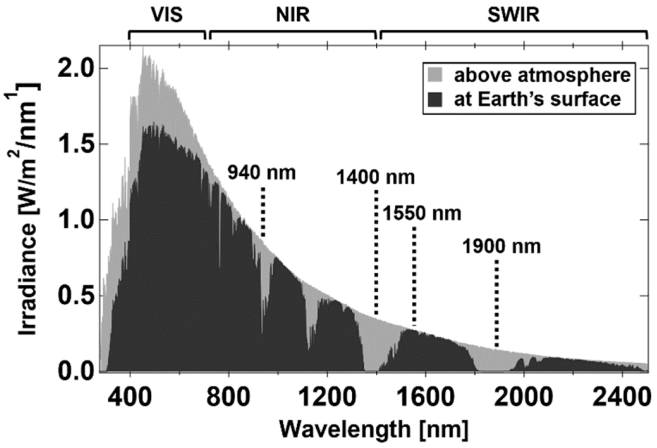

Fig. 1. Solar irradiance reaching the Earth, with some notable bands highlighted.

range (typically at 940 nm—Fig. 1), and in the mid-wave infrared (MWIR) range (3–5 μm), are also covered. Finally, an outlook on the future development, potential directions, and challenges to be solved is given. In order to help readers in understanding the content of this review, an appendix on colloidal QDs (CQDs), surface chemistry, and solution-based fabrication is given, which are the topics fundamental to this technology.

II. Overview of Technology Development

The first demonstrations of infrared photodetection with nanocrystals were reported early 2000s, starting with an article in 2004 by the Sargent Group (University of Toronto) [14]. In this work, an infrared-sensitive photoconductor was fabricated by integrating lead sulfide (PbS) nanocrystals in a polymer matrix which facilitated charge carrier extraction from the absorbing QDs. This solution-processed sensor with a sensitivity of up to 1300 nm heralded a new era and opened a path for the future low cost, high-resolution infrared image sensors, as an alternative to commercial and well-established solutions based on compound semiconductors. In less than five years, the first solution-processed infrared image sensor was demonstrated by Siemens [15], based on a thin-film photodiode with polymer-PbS blend as an absorber. Since then, a tremendous progress in infrared thin-film photodetectors has been achieved. To this date, PbS QDs remain the most exploited material for nanocrystal-based SWIR imaging.

Initially, this research was driven by photovoltaic groups, who mainly focused on QDs with the absorption onset in the visible and NIR range, optimal for light harvesting. Despite the improvements and the achieved power conversion efficiency of above 13% [16], the interest for QDs for photovoltaic applications is fading as more promising alternatives are emerging [17]. However, as the only solution-processed material that can offer competitive sensitivity at wavelengths above 1000 nm, QDs reign supreme in the infrared imaging domain.

A wide range of techniques and device architectures such as photoconductors, photodiodes, and phototransistors have been invented to extract charges from QD absorbers [18], offering

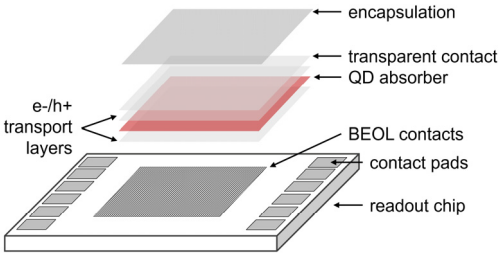

Fig. 2. Schematic representation of different layers of a QD-based image sensor.

a rich pool of viable solutions for integration with CMOS circuitry (Fig. 2). Organic semiconductors, metal oxides, or 2-D materials are typically used as an interface to the electrodes and readout circuits, although a direct integration on silicon has been demonstrated [19]. In addition to the progress in device architectures, findings in the field of surface chemistry accelerated the maturity of QD-based photodetectors. Surface properties of QDs, which depend on the material synthesis, but also on the ligands—molecules that bind to QD surface—are crucial for obtaining desirable design parameters. By optimizing the ligand layer on the surface of QDs, researchers improved properties, such as carrier mobility, lifetime, and trap state density, and established a relatively good control over band energy levels and doping densities [20]–[22].

Significant progress in the development of image sensors based on QDs has been achieved on different frontiers. Recently, high EQE in SWIR of 80% measured on a single photodetector [23] and 40% measured on a pixel array [24] have been demonstrated, which strongly suggests that this technology can be a viable alternative to FPAs based on compound semiconductors. In terms of fabrication, photolithographic patterning of QD films was successfully performed [25]. In addition, an inkjet-printing (IJP) process has been developed as an alternative to commonly used spin coating, which could facilitate wafer-level fabrication and upscaling of this technology [26]. In terms of resolution and pixel density, image sensors based on CQDs have already outperformed InGaAs FPAs, with large arrays of 1920 px $\times$ 1080 px available on the market [27] and demonstrated pixel pitch of 1.1 μm [28] and 1.82 μm [29] for NIR and SWIR, respectively. Finally, recently reported response time of 10 ns for PbS [23] and sub-1 ns for InAs QDs [30] is promising results for achieving affordable time-of-flight imaging solutions in SWIR.

III. QD-Based Image Sensors

The key results achieved in the field of QD-based infrared imaging are presented in this section. Operation principles and different approaches adopted by various companies and research groups are covered. The section is divided into three parts: Section III-A dedicated to PbS QDs as the material of choice for most of the groups working in this field, Section III-B is dedicated to mercury telluride (HgTe) QDs that have been demonstrated as a viable option as well, and Section III-C briefly touches on potential alternative QDs that

Authorized licensed use limited to: Biruni Universitesi. Downloaded on November 13,2022 at 13:03:58 UTC from IEEE Xplore. Restrictions apply.

Fig. 3. Representative images made by different QD image sensors. (a) PbS QD, SWIR image (cutoff at 1.6 μm), 5-μm pixel pitch, and data courtesy of IMEC. (b) PbS QD, SWIR image (cutoff at 2 μm), 15-μm pixel pitch, and data courtesy of SWIR vision systems. (c) PbS QD, SWIR image (cutoff at 2 μm), 20-μm pixel pitch, and data courtesy of Emberion. (d) PbS QD, SWIR image (cutoff at 1.6 μm), 2.2-μm pixel pitch, and data courtesy of STMicroelectronics. (e) PbS QD, SWIR image (cutoff at 1.85 μm), and data courtesy of ICFO. (f) HgTe QD, MWIR image (cutoff at 5 μm), 30-μm pixel pitch, and reprinted with permission from [51]. (g) HgTe QD, SWIR image (cutoff at 2 μm), half VGA, 15-μm pixel pitch, and data courtesy of Sorbonne University.

have better prospects for a wider adoption from a toxicity and contamination point of view. Fig. 3(a)–(g) shows images made by QD-based image sensors, developed by different groups active in the field.

A. Infrared Image Sensors With PbS QDs

The most investigated thin-film material for infrared sensing and imaging is PbS QDs, which were utilized in various ways to achieve infrared imaging capability. This section is divided based on the implemented photodetector architecture and the accompanying readout method. The most common approach is a thin-film photodiode with PbS QDs as the absorber and additional thin-film transport layers made of metal oxides, organics, or 2-D materials, monolithically integrated on CMOS read-out integrated circuits (ROICs) of different kinds. Imaging with PbS QD-based phototransistors is another approach found in the literature, with fewer reports compared with the photodiode approach. Illustrations of common photodetector stacks and the corresponding band diagrams are given in Fig. 4. The spectral range for PbS QD image sensors is typically from visible to SWIR (up to 1.7 μm). However, this material offers an attractive possibility for an extension to 2 μm and beyond, also known as extended SWIR (eSWIR), which cannot be detected by the standard InGaAs FPAs. Fig. 5 shows spectra with EQE measured from different image sensors with PbS QD absorbers, demonstrating the potential of this material.

The long-term stability of PbS QD SWIR photodetectors is a crucial step in the commercialization of this technology. In one study, devices were stressed under different environmental conditions while recording external quantum efficiency, dark current, and response time. It was shown [31] that IMEC's SWIR QD photodetectors can still perform well after a damp heat test, also known as 85/85 [exposure for 1000 h to 85 °C temperature and 85% relative humidity (RH)], simulating 20 years of moisture ingress into a given device [32]. Under these conditions, several parameter changes were observed: an increase of a factor 5 in the dark current (from 2×10^{-3} to 1×10^{-2} mA/cm^2), a decrease in EQE from 40% to 30% at the peak wavelength, and a slight reduction in response time from 11 to 9 μs. In a recent presentation [33], STMicroelectronics reports that their PbS NIR stacks (optimized for 940 nm)

Authorized licensed use limited to: Biruni Universitesi. Downloaded on November 13,2022 at 13:03:58 UTC from IEEE Xplore. Restrictions apply.

pass the lifetime specs for consumer electronics applications [>400-h high-temperature stability for 125 °C/dry; >500-h thermal heat soak at 85 °C/85% RH; >500 cycles of thermal cycling from −40 °C to +125 °C; >60-h unbiased highly accelerated stress test (uHAST) at 110 °C/85% RH; 1600 h of high-temperature operating life (HTOL) at 70 °C in darkness; and >50 h of HTOL at 70 °C and illuminated with 1 W/m^2]. Further exploration into the degradation mechanisms of these devices is ongoing with the aim of better understanding the weak links in the devices. These first results encourage careful optimism as to relevance of SWIR QD stacks in real products and form a base for further improvements of their stability in harsh conditions.

1) Photodiodes With CTIA Readout: A fast and efficient approach for developing QD-based SWIR image sensors was demonstrated by Research Triangle Institute (RTI) International, whose spin-off SWIR Vision Systems released a first commercial product based on PbS QDs—the "Acuros1920" image sensor with 1920 × 1080 pixel array, outperforming InGaAs FPAs in terms of the array size [34]. They leveraged ROICs developed for detectors based on other material systems by monolithic integration of PbS QDs layers, effectively avoiding the difficulties associated with epitaxial growth of compound semiconductors and flip-chip hybridization process. A clear advantage of this approach is the rapid development that is enabled by using off-the-shelf ROICs, without a necessity to develop a dedicated pixel architecture.

SWIR Vision Systems used a heterojunction photodiode created by a PbS absorber and C60 as an electron transport layer (ETL), originally developed for photovoltaic applications [35]. The built-in field at the interface between these two materials serves to separate electron–hole pairs generated in the absorber. One of the advantages of this device design is that the same heterojunction can be used even for eSWIR [36].

A ROIC based on CTIA allows operation at a very low reverse bias, which is the approach adopted by SWIR Vision Systems [37]. CTIA pixel architecture normally includes one capacitor, a current source, two amplifiers, and two transistors (reset and row selector) [38]. Due to a high number of surface trap states of QDs, relatively high levels of dark current are reported in the literature. Hence, the operation with no or very little external bias is undoubtedly an effective method to minimize noise levels.

In their early work, SWIR Vision Systems demonstrated that PbS-C60 heterojunction can offer dark current comparable with that of commercial InGaAs photodiodes, with current densities of 2.7 nA/cm^2 at room temperature when biased at 10 mV [39]. However, in the same work, the demonstrated EQE at 1550 nm was below 10%, significantly lower compared with InGaAs (>80%). Nevertheless, in combination with the low dark current, this EQE proved to be sufficient for imaging with high sensitivity in SWIR. Then, they integrated the PbS-C60 heterojunction photodiode on a 640 × 512 pixel array with 15-μm pixel pitch, designed for InGaAs photodiodes. The image sensor exhibited dark current of 8 nA/cm^2 at room temperature, EQE of 14.5% at 1550 nm, and pixel yield above 99% (2σ) [40]. An important consideration when integrating QDs on ROICs is the flatness of the surface on which QDs are spin-coated. When an off-the-shelf ROIC is used, an additional planarization step might be necessary [40]. The arrayed electrodes on the ROIC, originally designed for bonding with a photodiode array chip, in this case, serve not only to readout signals from thin-film absorption but also to boost EQE, a common approach in the thin-film photodiode design. Hence, high optical reflection is another factor that requires an engineered surface. Recently, SWIR Vision Systems demonstrated a test photodiode array with optimized 40% EQE at 1500 nm (Fig. 5) [41].

Advancements in the field of PbS thin-film photovoltaics, with several examples of solar cells reported in the literature exhibiting EQE of 80% in SWIR [42], [43], provide a great opportunity for the development of high-performance SWIR image sensors based on CTIA readout architecture and low bias voltage. However, by using the ROICs intended for traditional infrared FPAs, the pixel density remains limited by the design optimized for the flip-chip hybridization process. Hence, even with a dedicated ROIC development, a low pixel pitch remains a challenge due to the complexity of CTIA architecture that requires a large chip footprint. SWIR Vision Systems demonstrated a ROIC design based on CTIA architecture with 3-μm pixel pitch [37]. Although this pitch is relatively large compared with commercial CISs, it is lower than pixel pitch of the state-of-the-art InGaAs-based devices. Advanced technology nodes can enable further scaling of CTIA engines.

2) Photodiodes With 3T Readout: Infrared image sensors with very high pixel density can be achieved if QD photodiodes are integrated on a dedicated ROIC employing a compact 3T pixel architecture. Such design contains three transistors: reset, row select, and a source follower [44], and requires significantly less space on a chip compared with CTIA. Moreover, this type of readout consumes less power. The 3T approach resembles commercial CISs, and pixel pitch is limited either by CMOS node technology or fundamentally by light diffraction, and not by integration issues such as flip-chip hybridization. By adopting this approach, InVisage demonstrated a 1.1-μm pixel pitch image sensor using PbS QDs for NIR [28], and IMEC demonstrated a pixel pitch of 1.82 μm for SWIR, also using PbS QDs [29]. A clear disadvantage of 3T readout for QD image sensors is the required voltage swing on a photodiode of a few 100 mV to 1 V, which inevitably causes an increase in the dark current. Unlike the photodetectors operating at close-to-zero bias, the reported photodetectors integrated with 3T readouts typically have a sharp drop in EQE at low biases, which allows them to be shut off simply by controlling the bias voltage, enabling global shutter operation [28].

Recently, heterojunction and homojunction PbS QD photodiodes were compared in combination with a 3T readout [24]. The heterojunction photodiode, which consists of an n-type ETL and a p-type PbS layer, exhibited a low dark current of 20 nA/cm^2 at −1-V bias, measured at room temperature, but rather low EQE of 12%. In contrast, the homojunction design, based on a wider n-type and a short p-type PbS layer, exhibited higher dark current of 780 nA/cm^2 under the same conditions, but high EQE of 40% at 1450 nm (Fig. 5). Moreover, the

Authorized licensed use limited to: Biruni Universitesi. Downloaded on November 13,2022 at 13:03:58 UTC from IEEE Xplore. Restrictions apply.

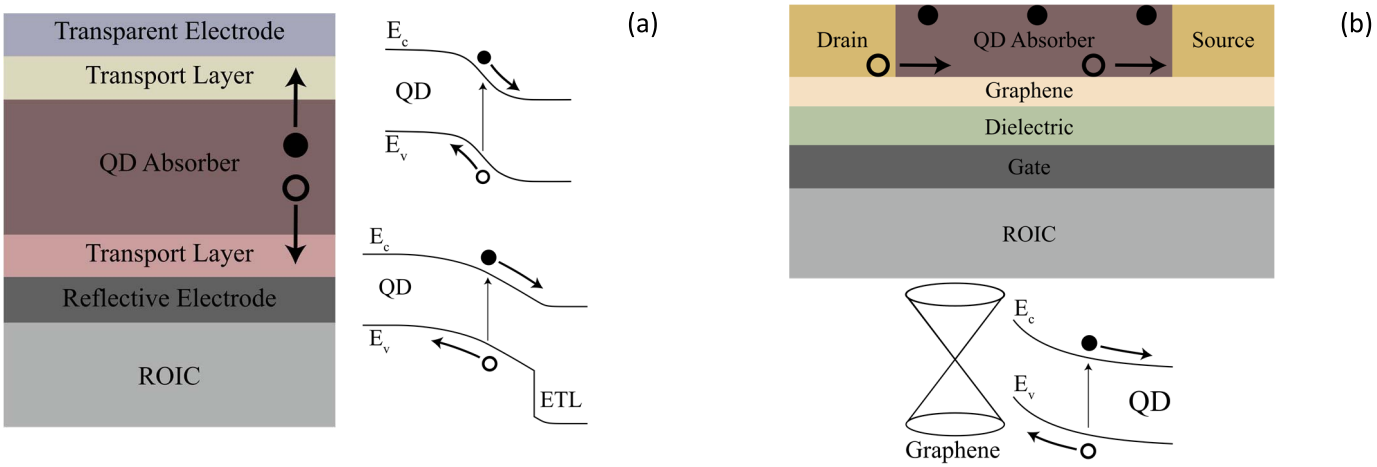

Fig. 4. Schematic photodetector stacks and band diagrams of commonly used QD photodetectors. (a) Thin-film photodiode with a QD absorber integrated on a ROIC. Electrons (solid circles) and holes (empty circles) are separated by an internal electric field and driven toward the opposite ends of the stack via transport layers. The photodiode can be fabricated in a form of a homojunction (upper diagram) or in a form of a heterojunction (bottom diagram) using one of the transport layers (e.g., ETL) to deplete the QDs. (b) Thin-film phototransistor with QD absorber and graphene as a transport layer integrated on a ROIC. In the illustrated device structure, electrons are trapped at QDs, while holes are injected from contacts and circulate via graphene layer, causing the photoconductive gain. The corresponding band diagram is given below.

homojunction performed better in terms of linearity, which is highly desirable for the 3T operation and image quality. The homojunction, which is fabricated by using distinct ligands in the ligand exchange process and consists dominantly of n-type PbS films due to their higher mobility, was studied as a promising option for PbS solar cells. However, little attention has been paid to the dark current mechanisms of this type of device. Indeed, the attention was focused on optimizing the bandgap for maximum light harvesting. Due to the differences in the crystal shape and surface chemistry between QDs of different sizes, i.e., different bandgaps, deeper investigation of trap states and surface chemistry is needed, which could eventually lead to a decrease in the dark current.

STMicroelectronics recently announced their work on NIR and SWIR image sensors that will feature global shutter operation, low pixel pitch of 2.2 and 1.62 μm, and EQE of 60% in SWIR (Fig. 5) [33]. This suggests that they implemented the photodiode with 3T readout approach, although other possible approaches cannot be ruled out. At the moment of writing this review article, STMicroelectronics is the only established semiconductor manufacturing company that is openly active in this field, and its activities validate the potential of upscaling of this technology. The pixel pitch of 1.62 μm, to be published while this review is in the publication process, sets the new state of the art in SWIR pixel density [45].

3) Photodiodes With Open-Circuit Voltage Readout: A third approach employing photodiodes for SWIR imaging has been shown by Emberion, a startup that commercializes QD image sensor technology. They released the Emberion VS20 camera with VGA resolution (640 × 512 array size) operating in 400–2000-nm wavelength range (Fig. 5) and with 20-μm pixel pitch [46]. The difference in their approach compared with the previous two is the readout method based on the open-circuit voltage mode [47]. Pixel structure is similar to a 3T pixel, but the photodiode is reset to be biased at 0 V and then floated, and the steady-state potential when the photocurrent becomes equal to the forward current is read out. With this readout method, the dark current noise can be effectively eliminated, and high dynamic range can be achieved. Moreover, thanks to its relatively simple structure and the small chip footprint required, open-circuit voltage readout gives a possibility to design an image sensor with a small pixel pitch. On the negative side, open-circuit voltage readout is characterized by pixel-to-pixel nonuniformities and a high-temperature sensitivity, which can result in a higher system cost and complexity due to a cooling system that might be necessary. In their article [46], Emberion reported EQE of 20% at 1550 nm, which, as they claim, in combination with the low noise performance, satisfies many applications. In addition to the p-i-n photodiode architecture which is the base of their current commercial product, they are also developing a Schottky photodiode, which is expected to give low saturation current, and a phototransistor, both characterized by having a graphene layer as a part of the sensor stack. Despite its positive effects on the overall performance, issues regarding fabrication and sensitivity can arise by the inclusion of graphene in the photodetector stack.

4) Phototransistors With CTIA Readout: Another imaging approach found in the literature is based on a phototransistor employing QDs as an absorber and graphene to enhance carrier transport. In addition to the work in this direction presented by Emberion, this approach was adopted by the The Institute of Photonic Sciences (ICFO) research institute, who recently spun off this work in a company QURV. In 2017, ICFO demonstrated a 388 × 288 imaging array for SWIR, based on PbS QD-graphene phototransistors [48]. The principle of operation of this device is based on a photogating effect that induces gain, leading to responsivity values as high as 10^7 AW^{-1}. When incident photons generate electron–hole pairs, electrons remain trapped at QDs, while holes are transferred to graphene. As long as electrons remain trapped, holes are injected from the electrodes and

Authorized licensed use limited to: Biruni Universitesi. Downloaded on November 13,2022 at 13:03:58 UTC from IEEE Xplore. Restrictions apply.

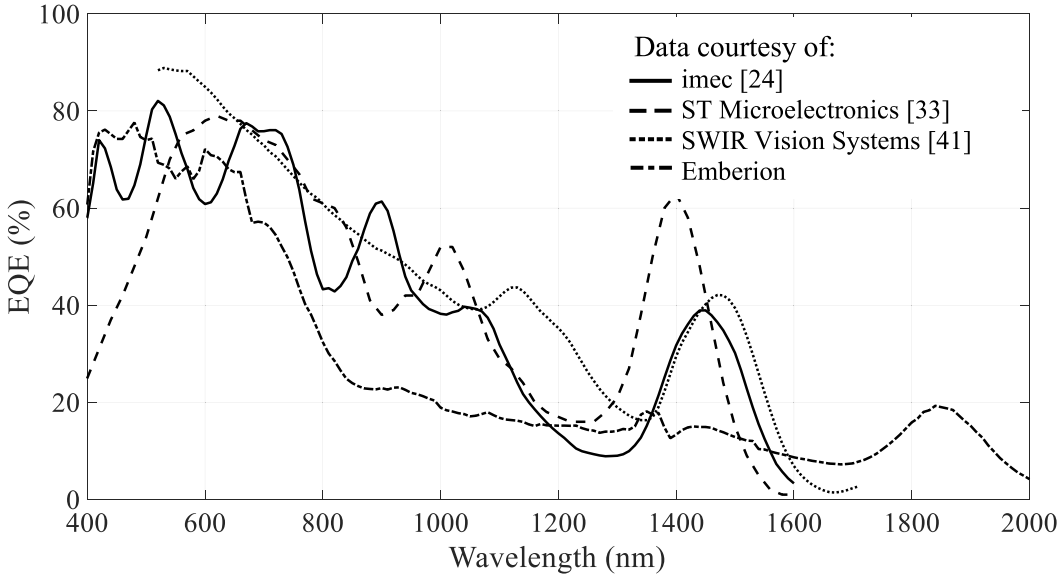

Fig. 5. Representative EQE spectra measured from different PbS QD image sensors for the SWIR range. All four image sensors exhibit high EQE in SWIR at the position of the excitonic peak, defined by the QD size. The characteristic troughs and peaks originate from the optical interference in the thin films. Unlike standard InGaAs FPAs, QD image sensors have broadband response with high EQE in the visible range.

circulate through the graphene layer [Fig. 4(b)]. Hence, as per single-absorbed photon, there are multiple holes collected, leading to photoconductive gain [49]. The authors demonstrated that this type of device in combination with CTIA-based readout can be used to capture images in SWIR. Operation with high gain can enable detection of very low light signals. At the same time, carrier trapping can compromise the speed of operation due to the necessary time to discharge the trapped electrons, which is problematic for applications requiring a fast response. Voltage- and light-dependent nonlinearities, pixel-to-pixel gain variation, and temperature-dependent gain variation in such devices pose a challenge for the readout design and system complexity.

From the integration point of view, high-gain phototransistors allow for deposition of thin absorbers (<100 nm), since the signal dominantly originates from hole circulation via injection from electrodes and even low absorption path can lead to a high signal. In the previous examples with photodiodes, absorbers of several 100 nm are necessary to obtain sufficiently high EQE, which can be challenging to fabricate (see Appendix). Hence, by using phototransistors, this issue can be avoided. Potential spread in pixel sensitivity due to nonuniformity in the graphene layer can be compensated by adding a variable resistor in the pixel circuit [48].

Table I summarizes key figures of merit of five different PbS QD image sensors based on different ROIC types and/or photodetector structures.

B. Image Sensors With HgTe QDs

Whereas all the previous examples are based on PbS QDs, alternative QD materials are also considered for low-cost infrared imaging. IR-absorbing HgTe QDs were successfully integrated on readout arrays, in a similar fashion to their PbS counterparts. A feature that makes HgTe QDs stand out is their wide bandgap tunability. Photodetectors with HgTe absorbers for SWIR, MWIR, and even long-wave infrared (LWIR) were demonstrated [50], which significantly exceeds the capabilities of PbS QDs in this regard.

Buurma *et al.* [51] demonstrated a 320 × 256 FPA with HgTe QDs integrated on top of a ROIC with 30-μm pixel pitch operating in MWIR wavelength range of 3–5 μm. Despite the low median EQE of 0.64%, noise equivalent differential temperature (NEDT) of 102 mK at 100 K was achieved thanks to the low noise, which allowed capturing of high-quality images and videos in MWIR. Moreover, smaller HgTe with a cutoff at 1.7 μm have been demonstrated on a 549 × 254 pixels readout array, proving that these QDs can be used for SWIR imaging as well [52].

Similar to PbS QDs, different types of photodetectors based on HgTe have been demonstrated, including photoconductors, photodiodes, and phototransistors [53]. Recently, HgTe-based photodiodes with 45% EQE at 4.5 μm have been demonstrated [54]. Moreover, their versatility was demonstrated with various devices such as multispectral and hyperspectral photodetectors [55], [56], and hybrid devices with silicon and graphene [57]. However, toxicity of Hg and contamination issues are the major bottlenecks for a wider adoption of this material and a potential upscaling that could lead to mass production of low-cost infrared image sensors. Nevertheless, HgTe QDs are still very attractive as a low-cost alternative for MWIR and LWIR applications.

C. Alternative QDs

Despite their potential and recent success in delivering low-cost infrared image sensors, PbS and HgTe QDs have one common major drawback, which is toxicity of their constituent atoms and contamination issues that might be a significant obstacle toward their introduction into CMOS foundries. Alternatives should be sought among materials with a very narrow

Authorized licensed use limited to: Biruni Universitesi. Downloaded on November 13,2022 at 13:03:58 UTC from IEEE Xplore. Restrictions apply.

TABLE I
FIGURES OF MERIT OF FIVE DIFFERENT PbS QD IMAGE SENSORS

Parameter	imec [24]	SWIR V.S. [34]	STM [45]	Emb. [46]	ICFO [48]	Unit
Pixel pitch	5	15	1.62	20	na	µm
Resolution	768x512	1920x1080	0.9 MPx	640x512	388x288	px
CG	2.2	na	52	na	na	$\mu V/e^-$
DR	82	70	53.4	120	>80	dB
V_{SWING}	0.7	na	0.52	0.2	na	V
FWC	325	na	10	na	na	Ke^-
J_D	3.3 (@RT)	na	0.25 (@60C)	na	na	$\mu A/cm^2$
RN	25	<210	21.3	na	na	e^-
PRNU	2.4	na	1.4	na	na	%
λ_{PEAK}	1450	1470	1400	1850	1670	nm
EQE	40	15	60	20	$R=10^7\ AW^{-1}$	%

***CG**: conversion gain; **DR**: dynamic range; V_{SWING}: photodiode swing; **FWC**: full-well capacity; J_D: dark current density; **RN**: read noise; **PRNU**: photo-response non-uniformity; λ_{PEAK}: peak wavelength; **EQE**: external quantum efficiency;*
***SWIR V.S.**: SWIR Vision Systems Inc.; **STM:** ST Microelectronics; **Emb.:** Emberion Oy; **ICFO:** The Institute of Photonic Sciences*

bandgap in their bulk form (absorption onset in MWIR or LWIR) such as InAs or InSb, which leave enough room for spectral tuning via nanocrystal size-engineering. InAs have recently attracted attention as a potential alternative to PbS for NIR photodetection and imaging with single photodetectors exceeding 30% EQE at 940 nm [30]. Especially attractive is the low dielectric constant of InAs QDs which gives a possibility to reduce the time response of the photodetectors thanks to the lower *RC* constant of InAs films. Fast sub-1-ns response time of InAs QD NIR photodetectors [30] gives a hope that QDs could be used for affordable infrared time-of-flight applications in the future. First, SWIR devices and their integration on readout arrays are yet to be demonstrated, while SWIR-absorbing InAs QDs have been already successfully synthesized [58]. In order to successfully integrate any new QDs into optoelectronic devices, a good understanding of their surface properties is needed. Moreover, a good control of the synthesis routes is necessary to fully leverage the available spectral range. Recent works on these topics [58], [59] are of high importance for the future development of InAs photodetectors and image sensors.

D. Comparison of Monolithic QD Image Sensors to Hybrid FPAs

In this article, we introduced monolithic CQD image sensors, and then compared and discussed various implementations adopted by different academic groups and companies. The technology is gaining momentum and a question arises whether it can rival the traditional hybrid FPAs for infrared imaging. A clear advantage of QD image sensors over their III–V counterparts is the potential for fabrication upscaling which is enabled by the monolithic integration of thin-film photodetectors on CMOS ROICs. Consequently, their price is expected to be significantly lower. Moreover, the monolithic integration removes the resolution constraints associated with hybrid III–V FPAs.

Photodetectors based on III–V materials such as InGaAs, the most common material for the SWIR range, are mature, exhibit high EQE of 80% [7] and dark current lower than 1 nA/cm^2 [6], and can be used for high-speed single-photon avalanche diodes (SPADs) [60]. As shown in Section III-A, PbS QD image sensors can already reach EQE values of 60% [33], with a prospect of reaching 80% in the future, as demonstrated by several photodetectors and solar cells reported in the literature [42], [43]. Moreover, with the right readout method, dark current measured in single digits of nA/cm^2 at room temperature can be reached [39]. Hence, QD image sensors have a potential to match InGaAs FPAs in terms of detectivity.

One feature of the QD image sensors is the characteristic spectral shape with peaks and throughs originating from the optical interference in thin films, which can limit their usage for applications that require high and stable EQE over a broad spectral range. In contrast, QD image sensors are characterized by a broadband response starting in the visible range and a wide bandgap tunability which makes even MWIR and LWIR ranges easily accessible.

Regarding the speed of operation, essential issue for time-of-flight applications, low mobility of QD absorbers makes them inferior to bulk semiconductors. Several important achievements on this frontier were achieved [23], [30], but it is still early to say whether these materials will be able to compete with conventional III–V technologies for applications that require fast operation. Most likely, certain tradeoffs in the performance will probably have to be made to enable time-of-flight applications with QD absorbers. We believe that III–V FPAs will remain dominant for high-end applications with

Authorized licensed use limited to: Biruni Universitesi. Downloaded on November 13,2022 at 13:03:58 UTC from IEEE Xplore. Restrictions apply.

stringent requirements, whereas QD image sensors can penetrate less-demanding markets which prioritize affordability, compactness, and high pixel density.

IV. Application Examples

In this paragraph, we enumerate the use cases covered by different groups in their research articles and conference presentations. These show the early demonstrations of capability of QD imagers for the SWIR range.

1) Defect inspection in bonded silicon wafers.
2) Through-wafer visualization of alignment markers.
3) Low-light passive imaging (night vision).
4) Imaging in adverse weather conditions (haze, dust, fog, mist, smoke, rain, and snow) in marine and automotive systems.
5) Detection of liquid levels through nontransparent plastic bottles.
6) Evaluation of fruit ripeness and detection of bruises.
7) Moisture detection on food products.
8) Visualization of food products through nontransparent packaging.
9) Pharmaceutical inspection in vials through plastic labels.
10) Food sorting (coffee beans with unwanted stones and plastic elements; recognition of powders and liquids that look the same in the visible range).
11) Plastic sorting (recognition of different types of plastics).
12) Counterfeit money recognition (ink contrast, hidden features).
13) High-resolution thermal inspection (bottle production).
14) Chip defect inspection (crack detection inside/outside of silicon).
15) Art inspection with reflectography.
16) Lens-free microscopy (computational imaging of microchannels through silicon wafer).
17) Laser beam visualization.
18) Through-sunglasses vision (security cameras, in-cabin monitoring for automotive).
19) Aerial imaging (drone-based).

These examples illustrate the breadth of application cases for SWIR imaging but also the fragmentation and specificity of different fields. The published articles highlight the advantages of QD-based sensors compared with InGaAs sensors. Smaller pixel pitch leads to recognition of finer spatial features [higher modulation transfer function (MTF)]. Higher resolution (number of pixels) enables the collection of more data points. Larger array size increases the field of view. All lead to higher image quality and the up-scalable manufacturing methods facilitate customization to fit each distinct use case.

V. Conclusion and Future Work

The inherent detectable wavelength limitation due to the bandgap of silicon sets the quest for alternative photo-active materials in the infrared domain. In this work, we provided the state-of-the-art overview of nanocrystalline materials that are directly processed on top of silicon ROICs. This combination ensures that the benefits of Si ROICs with all the downscaling in pixel pitch can be combined with thin-film infrared absorbing materials to create imagers with unprecedented specifications. First imagers are demonstrated, both based on CTIA readout for low-voltage operation, on 3T pixel readout scheme for small pixel pitch, on open-circuit voltage mode for high dynamic range, and also on phototransistors for gain-based operations. A lot of these imagers utilize the existing Si ROICs, for example, ROICs that are also used in combination with flip-chip bonded InGaAs photodetectors. At the same time, dedicated ROIC designs start appearing and are expected to grow in importance. Such approach will reveal the full potential enabled by the nanocrystalline thin-film absorber materials. Imagers with smaller pixels, going toward the range of standard CIS, will facilitate the incorporation of infrared imagers in applications such as consumer electronics and in applications where the current imagers are not suitable due to their form factor and cost. Furthermore, the fact that the nanocrystals can be monolithically processed on top of the ROIC empowers completely novel type of read-out schemes.

On the optical front, the use of thin-film layers creates an interference pattern inside the photoactive layer stack. As a result, each stack should be optimized in terms of complex index of refraction and thickness for the used metals, interlayers, and active layers. Most applications will require optical filters and/or microlenses integrated on top modules that are not well studied. These additional layers may alter the interference pattern, and this should be included in the optical design. Another potential route on the optical front is going to multispectral or even hyperspectral SWIR or MWIR line scanners or cameras. The monolithic processing of the thin-film layers on the ROIC will enable novel options on the multispectral front, such as the use of microcavities for spectral filtering.

The uptake of this novel technology into the industry is currently hampered by the lack of large scale, wafer-level processing. Most demonstrators discussed above are based on liquid processing of QDs on top of dies (coupon level—parts of a wafer). Challenges lay in a uniform, agglomeration-free deposition on a large surface (e.g., 200- or 300-mm silicon wafers). Some of the used stacks rely on multistep liquid deposition for QD ligand exchange, resulting in up to $\sim$30 steps for a single layer. A single deposition step is much preferred in industry, where a single QD ink is used, without later ligand exchange steps. Finally, the use of toxic materials might block processing in semiconductor fabs, so research on this front will continue. The developments for Pb-free absorber materials might be compared with the route that the light-emitting QDs made in order to find Cd-free alternatives to the first emitters.

QD imagers have been gaining momentum, with both academic and industrial players setting a fast development pace. The most promising disruption seems to be the SWIR range, with pixel density unprecedented in incumbent sensors based on flip-chip integration. First technology validation is expected in specialized sectors, with scientific (microscopy) and industrial (inspection, sorting) as entry markets. At the same time, monolithic fabrication promises to make this technology affordable for many applications that could not

Authorized licensed use limited to: Biruni Universitesi. Downloaded on November 13,2022 at 13:03:58 UTC from IEEE Xplore. Restrictions apply.

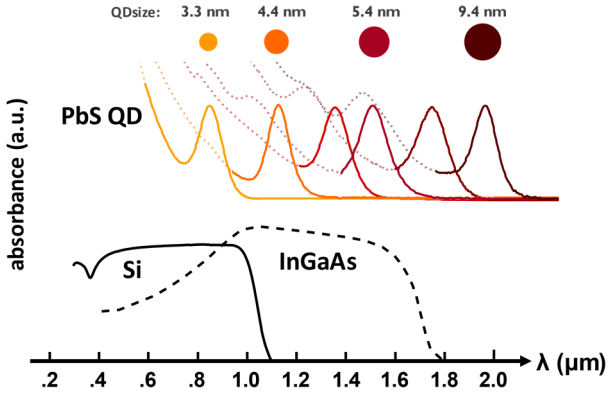

Fig. 6. Quantum size effect in PbS nanocrystals: tuning the size of the PbS QDs allows absorption of longer wavelength, outperforming existing silicon and InGaAs technologies.

have considered data acquisition in SWIR. This will open new machine vision segments, such as smart agriculture (tractor-, drone-, and robot-mounted sensors), medical (endoscopy), or surveillance (security cameras). Going further, smaller pixels (toward the range of standard CIS) will shrink the form factor and facilitate incorporation of SWIR cameras even in consumer applications. Here, examples are biometric identification (with lower background than in NIR), eye-safe eye-tracking (in augmented reality/virtual reality (AR/VR) head-mounted devices), or augmented vision (material recognition, seeing in the dark). Improving reliability of the QD imagers can finally result in market entry into the automotive sector. There, SWIR cameras can contribute to safety improvement both in outside camera systems (better visibility in adverse weather conditions) and in-cabin systems (both in dark and very bright conditions with a lot of background). Scaling the manufacturing to a foundry-compatible, wafer-level process will fuel new innovations and new implementations of QD-based image sensors.

APPENDIX
SURFACE CHEMISTRY OF CQDS

CQDs are nanosized particles of semiconductors, which are mostly famous for the size dependency of their optical properties. The wavelengths of their absorption and emission depend not only on the material from which the nanoparticle is made, but also on the size of the particle, through the quantum size effect (Fig. 6).

The effect of size on the physical and electronic properties of CQDs can be understood by looking at the theoretical treatment of such systems. Much of the basic physics of confined systems can be explained by the simple "particle in a box" model [61].

A. Synthesis of Semiconductor Nanocrystals

CQDs are usually synthesized via bottom-up approach in a solution. Based on this method, ionic precursors are swiftly injected into a hot solution containing surfactant molecules and additional precursors.

The growth mechanism of colloidal nanoparticles begins with the creation of small, discrete nucleation clusters, made

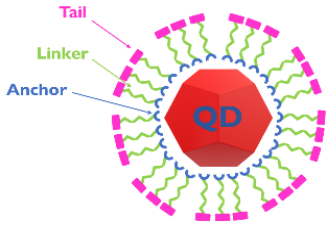

Fig. 7. Ligand is made of an anchor group, a spacer, and a tail group.

of several tens of atoms, followed by a controlled growth on these clusters.

1) Organic Surface Passivation—Ligands of Semiconductor Nanocrystals: In the pyrolytic synthesis approach, the resultant CQDs are covered by surfactant organic molecules, commonly known as ligands. Schematically, organic ligands can be described as made of three different parts: an anchor group, connected to the CQD surface, a spacer, and a tail group (Fig. 7), which faces outward and can be chemically functionalized, in order to render the CQD different properties, such as polarity, or allow further chemistry to take place, such as polymerization.

2) Ligand Exchange Processes: As mentioned, synthesized QDs come out of the synthesis vessel covered with long and insulating ligands. While these ligands serve well in stabilizing the colloidal solution and in passivating the CQDs surface, it is essential to replace them with shorter ligands that will allow better coupling between QDs and, therefore, better charge transport.

The efficiency of ligand exchange process, which takes place in a nonpolar solvent, is electrostatically limited to neutral ligands, because of the energetically unfavored solvation of a charged molecule in a nonpolar solvent. For this reason, L-type ligands (such as amines) would rapidly adsorb and desorb from the nanocrystal surface at room temperature, while X-type remain tightly bound.

Furthermore, the initial state of the original ligands packing is to be taken into consideration. Long-chained alkyl ligands would be more densely packed on the surface of the CQD and would assume a crystalline structure, while shorter chained ligands would be adsorbed in a more liquid-like phase [62]. Naturally, the more densely packed the original ligands are, the harder it would be to replace them.

B. Solution Processing

There are two main approaches for processing CQD for thin-film devices: layer-by-layer (LbL) approach and solution phase ligand exchange (SPLE) approach. In LbL, the ligand exchange step is done *in situ*, by using spin coating methods. LbL deposition is a relatively simple process, but it is tedious and wasteful, especially when thicker (>100 nm) films are needed. In SPLE, an ink is prepared in advance and can be deposited onto the device in several methods: spin coating, IJP, or spray coating. This approach offers a possibility to deposit thick films efficiently, but it can be challenging to prepare a stable QD ink following this method.

1) Spin Coating: In spin coating deposition, a small amount of the CQD solution is deposited on a substrate which is

Authorized licensed use limited to: Biruni Universitesi. Downloaded on November 13,2022 at 13:03:58 UTC from IEEE Xplore. Restrictions apply.

then quickly spun in order to create a uniform layer from the deposited solution. During spinning, centrifugal forces compress the solution into a thin layer, while the solvent evaporates, and excess material spins off the edges of the substrate. The eventual layer thickness depends (*inter alia*) on the spin speed, solution concentration, and solvent viscosity and volatility [55], [63].

2) Inkjet Printing: IJP is a drop-on-demand technology, in which very small drops of CQD solution are deposited on a well-defined area, e.g., a pixel [64]. For this process to work, the ligand exchange process is done separately, and the resultant solution is loaded into a printer cartridge for further printing. Well-passivated CQD and stable inks are required for the realization of CQD IJP. In addition, ink rheological properties such as viscosity, surface tension, boiling point, particle size, and concentration must be carefully controlled to enable optimal inkjet performance [26].

3) Spray Coating: Another method to produce CQD-layers with well-controlled thickness is spray coating. In this method, the films are deposited by the supersonic spraying technique, which facilitates the rapid evaporation of the solvent and the subsequent deposition of the CQD ink without requiring a postdeposition annealing treatment for solvent removal. A fine mist containing CQDs is atomized using pressurized nitrogen gas, creating micrometer sized droplets, which are deposited on the substrate. The film thickness can be readily controlled by varying the number of spraying sweeps made across the substrate [65].

REFERENCES

[1] A. Rogalski, "History of infrared detectors," *Opto-Electronics Rev.*, vol. 20, no. 3, pp. 279–308, Jan. 2012, doi: 10.2478/s11772-012-0037-7.

[2] Xenics. (2021). *Bobcat 320 SWIR Cameras*. Imaging & Machine Vision Europe. Accessed: Nov. 17, 2021. [Online]. Available: https://www.imveurope.com/press-releases/bobcat-320-swir-cameras

[3] *New Imaging Technologies. Low Price Point InGaAs SWIR Camera for R&D and Industrial Applications*. Accessed: Nov. 17, 2021. [Online]. Available: https://new-imaging-technologies.com/news/low-price-point-ingaas-swir-camera-for-rd-and-industrial-applications/

[4] J. F. Klem, J. K. Kim, M. J. Cich, G. A. Keeler, S. D. Hawkins, and T. R. Fortune, "Mesa-isolated InGaAs photodetectors with low dark current," *Appl. Phys. Lett.*, vol. 95, no. 3, Jul. 2009, Art. no. 031112, doi: 10.1063/1.3184807.

[5] P. Martyniuk and A. Rogalski, "HOT infrared photodetectors," *Opto-Electron. Rev.*, vol. 21, no. 2, pp. 239–257, Jan. 2013, doi: 10.2478/s11772-013-0090-x.

[6] R. Fraenkel *et al.*, "Development of low-SWaP and low-noise InGaAs detectors," in *Proc. 43rd Infr. Technol. Appl.*, vol. 10177, 2017, Art. no. 1017703, doi: 10.1117/12.2262112.

[7] A. Rouvié *et al.*, "InGaAs focal plane array developments and perspectives," in *Proc. 41st Infr. Technol. Appl.*, vol. 9451, 2015, Art. no. 945105, doi: 10.1117/12.2179986.

[8] W. Zhang *et al.*, "Fabrication of high aspect ratio bumps for focal plane arrays applications," in *Proc. Infr. Technol. Appl.*, 2019, Art. no. 110022F, doi: 10.1117/12.2519202.

[9] R. Fraenkel *et al.*, "High definition 10 μm pitch InGaAs detector with asynchronous laser pulse detection mode," in *Proc. 42nd Infr. Technol. Appl.*, vol. 9819, 2016, Art. no. 981903, doi: 10.1117/12.2222762.

[10] S. Manda *et al.*, "High-definition visible-SWIR InGaAs image sensor using Cu–Cu bonding of III–V to silicon wafer," in *IEDM Tech. Dig.*, Dec. 2019, pp. 7–16, doi: 10.1109/IEDM19573.2019.8993432.

[11] C.-C. Hsieh, C.-Y. Wu, F.-W. Jih, and T.-P. Sun, "Focal-plane-arrays and CMOS readout techniques of infrared imaging systems," *IEEE Trans. Circuits Syst. Video Technol.*, vol. 7, no. 4, pp. 594–605, Aug. 1997, doi: 10.1109/76.611171.

[12] A. Rogalski, *Quantum Dot Photodetectors*. Cham, Switzerland: Springer, 2021, doi: 10.1007/978-3-030-74270-6.

[13] M. Takase, Y. Miyake, T. Yamada, T. Tamaki, M. Murakami, and Y. Inoue, "First demonstration of 0.9 μm pixel global shutter operation by novel charge control in organic photoconductive film," in *IEDM Tech. Dig.*, Dec. 2015. [Online]. Available: https://ieeexplore.ieee.org/document/7409799?anchor=authors&signout=success, doi: 10.1109/IEDM.2015.7409799.

[14] S. A. McDonald, P. W. Cyr, L. Levina, and E. H. Sargent, "Photoconductivity from PbS-nanocrystal/semiconducting polymer composites for solution-processible, quantum-size tunableinfrared photodetectors," *Appl. Phys. Lett.*, vol. 85, no. 11, pp. 2089–2091, Sep. 2004, doi: 10.1063/1.1792380.

[15] T. Rauch *et al.*, "Near-infrared imaging with quantum-dot-sensitized organic photodiodes," *Nature Photon.*, vol. 3, no. 6, pp. 332–336, Jun. 2009, doi: 10.1038/nphoton.2009.72.

[16] M. Biondi *et al.*, "Control over ligand exchange reactivity in hole transport layer enables high-efficiency colloidal quantum dot solar cells," *ACS Energy Lett.*, vol. 6, no. 2, pp. 468–476, Feb. 2021, doi: 10.1021/acsenergylett.0c02500.

[17] J. Y. Kim, J.-W. Lee, H. S. Jung, H. Shin, and N.-G. Park, "High-efficiency perovskite solar cells," *Chem. Rev.*, vol. 120, no. 15, pp. 7867–7918, Aug. 2020, doi: 10.1021/acs.chemrev.0c00107.

[18] R. Saran and R. J. Curry, "Lead sulphide nanocrystal photodetector technologies," *Nature Photon.*, vol. 10, no. 2, pp. 81–92, Feb. 2016, doi: 10.1038/nphoton.2015.280.

[19] K. Xu *et al.*, "Inverted Si: PbS colloidal quantum dot heterojunction-based infrared photodetector," *ACS Appl. Mater. Interfaces*, vol. 12, no. 13, pp. 15414–15421, Apr. 2020, doi: 10.1021/acsami.0c01744.

[20] D. Zhitomirsky *et al.*, "N-type colloidal-quantum-dot solids for photovoltaics," *Adv. Mater.*, vol. 24, no. 46, pp. 6181–6185, Dec. 2012, doi: 10.1002/adma.201202825.

[21] O. Voznyy, D. Zhitomirsky, P. Stadler, Z. Ning, S. Hoogland, and E. H. Sargent, "A charge-orbital balance picture of doping in colloidal quantum dot solids," *ACS Nano*, vol. 6, no. 9, pp. 8448–8455, Sep. 2012, doi: 10.1021/nn303364d.

[22] P. R. Brown *et al.*, "Energy level modification in lead sulfide quantum dot thin films through ligand exchange," *ACS Nano*, vol. 8, no. 6, pp. 5863–5872, Jun. 2014, doi: 10.1021/nn500897c.

[23] M. Vafaie *et al.*, "Colloidal quantum dot photodetectors with 10-ns response time and 80% quantum efficiency at 1,550 nm," *Matter*, vol. 4, no. 3, pp. 1042–1053, Mar. 2021, doi: 10.1016/j.matt.2020.12.017.

[24] V. Pejovic *et al.*, "Thin-film photodetector optimization for high-performance short-wavelength infrared imaging," *IEEE Electron Device Lett.*, vol. 42, no. 8, pp. 1196–1199, Aug. 2021, doi: 10.1109/led.2021.3093081.

[25] E. Georgitzikis *et al.*, "Integration of PbS quantum dot photodiodes on silicon for NIR imaging," *IEEE Sensors J.*, vol. 20, no. 13, pp. 6841–6848, Jul. 2020, doi: 10.1109/JSEN.2019.2933741.

[26] R. Sliz *et al.*, "Stable colloidal quantum dot inks enable inkjet-printed high-sensitivity infrared photodetectors," *ACS Nano*, vol. 13, no. 10, pp. 11988–11995, Oct. 2019, doi: 10.1021/acsnano.9b06125.

[27] SWIR Vision Systems. *Acuros CQD 1920/1920L GigE SWIR Camera*. Accessed: Nov. 17, 2021. [Online]. Available: https://www.swirvisionsystems.com/wp-content/uploads/Acuros-CQD-1920L-GigE-SWIR-Camera_003.pdf

[28] Z. M. Beiley *et al.*, "Device design for global shutter operation in a 1.1-μm pixel image sensor and its application to near infrared sensing," in *Proc. 25th Phys. Simulation Optoelectronic Devices*, 2017, vol. 10098, Art. no. 100981L, doi: 10.1117/12.2253219.

[29] J. Lee *et al.*, "Imaging in short-wave infrared with 1.82 μm pixel pitch quantum dot image sensor," in *IEDM Tech. Dig.*, Dec. 2020, pp. 343–346, doi: 10.1109/IEDM13553.2020.9372018.

[30] B. Sun *et al.*, "Sub-nanosecond infrared photodetection using III-V colloidal quantum dots," *Res. Square*, 2020, doi: 10.21203/rs.3.rs-92318/v1.

[31] I. Lieberman, "Realizing high quality QD-based infrared image sensors based on quantum dot pixel stacks," in *Phosphors & Quantum Dots Industry Forum*. Smithers, 2021. [Online]. Available: https://www.photonicconference.com/home

[32] JEDEC. (Nov. 17, 2021). *JEDEC Standard No. 22-A101*. Accessed: Nov. 17, 2021. [Online]. Available: https://www.jedec.org/

[33] J. S. Steckel, A. G. Pattantyus-Abraham, E. Josse, E. Mazaleyrat, and K. Rochereau, "66-1: High resolution quantum dot global shutter imagers," in *Proc. SID Symp. Dig. Tech. Papers*, May 2021, vol. 52, no. 1, pp. 975–977, doi: 10.1002/sdtp.14852.

Authorized licensed use limited to: Biruni Universitesi. Downloaded on November 13,2022 at 13:03:58 UTC from IEEE Xplore. Restrictions apply.

[34] SWIR Vision Systems. *Acuros CQD 1920/1920L GigE SWIR Camera*. [Online]. Available: https://www.swirvisionsystems.com/wp-content/uploads/Acuros-CQD-1920L-GigE-SWIR-Camera_003.pdf

[35] E. J. D. Klem, C. W. Gregory, G. B. Cunningham, S. Hall, D. S. Temple, and J. S. Lewis, "Planar PbS quantum dot/C60 heterojunction photovoltaic devices with 5.2% power conversion efficiency," *Appl. Phys. Lett.*, vol. 100, no. 17, Apr. 2012, Art. no. 173109, doi: 10.1063/1.4707377.

[36] S. Hinds, E. Klem, C. Gregory, A. Hilton, G. Hames, and K. Violette, "Extended SWIR high performance and high definition colloidal quantum dot imagers," in *Proc. Infr. Technol. Appl.*, May 2020, Art. no. 1140707, doi: 10.1117/12.2559115.

[37] A. I. D. Souza *et al.*, "ROIC for 3 μm pixel pitch colloidal quantum dot detectors," in *Proc. Image Sens. Technol., Mater., Devices, Syst., Appl.*, vol. 10656, May 2018, Art. no. 1065614, doi: 10.1117/12.2315622.

[38] B. A. Fowler, J. Balicki, D. How, and M. Godfrey, "Low-FPN high-gain capacitive transimpedance amplifier for low-noise CMOS image sensors," in *Proc. 2nd Sensors Camera Syst. Sci., Ind., Digit. Photography Appl.*, vol. 4306, 2001, pp. 68–77, doi: 10.1117/12.426991.

[39] E. J. D. Klem, C. Gregory, D. Temple, and J. Lewis, "PbS colloidal quantum dot photodiodes for low-cost SWIR sensing," in *Proc. 41st Infr. Technol. Appl.*, vol. 9451, Jun. 2015, Art. no. 945104, doi: 10.1117/12.2178532.

[40] E. J. D. Klem, C. W. Gregory, D. S. Temple, and J. S. Lewis, "Colloidal quantum dot Vis-SWIR imaging: Demonstration of a focal plane array and camera prototype (presentation recording)," in *Proc. Opt. Sens., Imag., Photon Counting, Nanostructured Devices Appl.*, vol. 9555, 2015, Art. no. 955505, doi: 10.1117/12.2190372.

[41] C. Gregory, A. Hilton, K. Violette, and E. J. D. Klem, "66-3: Invited paper: Colloidal quantum dot photodetectors for large format NIR, SWIR, and eSWIR imaging arrays," in *Proc. SID Symp. Dig. Tech. Papers*, May 2021, vol. 52, no. 1, pp. 982–986, doi: 10.1002/sdtp.14854.

[42] Y. Bi, S. Pradhan, S. Gupta, M. Z. Akgul, A. Stavrinadis, and G. Konstantatos, "Infrared solution-processed quantum dot solar cells reaching external quantum efficiency of 80% at 1.35 μm and J_{sc} in excess of 34 mA cm^{-2}," *Adv. Mater.*, vol. 30, no. 7, Feb. 2018, Art. no. 1704928, doi: 10.1002/adma.201704928.

[43] J. Z. Fan *et al.*, "Mixed lead halide passivation of quantum dots," *Adv. Mater.*, vol. 31, no. 48, Nov. 2019, Art. no. 1904304, doi: 10.1002/adma.201904304.

[44] E. R. Fossum, "Active pixel sensors: Are CCD's dinosaurs?" in *Proc. SPIE, Int. Soc. Opt. Eng.*, vol. 1900, 1993, pp. 2–14.

[45] J. Steckel *et al.*, "1.62 μm global shutter quantum dot image sensor optimized for near and shortwave infrared," in *IEDM Tech. Dig.*, Dec. 2021, pp. 23–24.

[46] M. Allen, A. Bessonov, and T. Ryhänen, "66-4: Invited paper: Graphene enhanced QD image sensor technology," in *Proc. SID Symp. Dig. Tech. Papers*, vol. 52, no. 1, 2021, pp. 987–990, doi: 10.1002/sdtp.14855.

[47] R. Fragasse *et al.*, "Signal and noise analysis of an open-circuit voltage pixel for uncooled infrared image sensors," *IEEE Trans. Circuits Syst. I, Reg. Papers*, vol. 68, no. 5, pp. 1827–1840, May 2021, doi: 10.1109/TCSI.2021.3068595.

[48] S. Goossens *et al.*, "Broadband image sensor array based on graphene–CMOS integration," *Nature Photon.*, vol. 11, no. 6, pp. 366–371, Jun. 2017, doi: 10.1038/nphoton.2017.75.

[49] G. Konstantatos *et al.*, "Hybrid graphene–quantum dot phototransistors with ultrahigh gain," *Nature Nanotechnol.*, vol. 7, no. 6, pp. 363–368, Jun. 2012, doi: 10.1038/nnano.2012.60.

[50] C. Buurma, A. J. Ciani, R. E. Pimpinella, J. S. Feldman, C. H. Grein, and P. Guyot-Sionnest, "Advances in HgTe colloidal quantum dots for infrared detectors," *J. Electron. Mater.*, vol. 46, no. 11, pp. 6685–6688, Nov. 2017, doi: 10.1007/s11664-017-5720-5.

[51] C. Buurma, R. E. Pimpinella, A. J. Ciani, J. S. Feldman, C. H. Grein, and P. Guyot-Sionnest, "MWIR imaging with low cost colloidal quantum dot films," in *Proc. Opt. Sens., Imag., Photon Counting, Nanostructured Devices Appl.*, 2016, vol. 9933. [Online]. Available: https://spie.org/Publications/Proceedings/Paper/10.1117/12.2239986?SSO=1, doi: 10.1117/12.2239986.

[52] A. Chu *et al.*, "HgTe nanocrystals for SWIR detection and their integration up to the focal plane array," *ACS Appl. Mater. Interfaces*, vol. 11, no. 36, pp. 33116–33123, Sep. 2019, doi: 10.1021/acsami.9b09954.

[53] B. Martinez *et al.*, "Designing photovoltaic devices using HgTe nanocrystals for short and mid-wave infrared detection," *Phys. Status Solidi A*, vol. 217, no. 5, Mar. 2020, Art. no. 1900449, doi: 10.1002/pssa.201900449.

[54] X. Tang, M. M. Ackerman, and P. Guyot-Sionnest, "Thermal imaging with plasmon resonance enhanced HgTe colloidal quantum dot photovoltaic devices," *ACS Nano*, vol. 12, no. 7, pp. 7362–7370, Jul. 2018, doi: 10.1021/acsnano.8b03871.

[55] X. Tang, M. M. Ackerman, and P. Guyot-Sionnest, "Acquisition of hyperspectral data with colloidal quantum dots," *Laser Photon. Rev.*, vol. 13, no. 11, Nov. 2019, Art. no. 1900165, doi: 10.1002/lpor.201900165.

[56] X. Tang, M. M. Ackerman, M. Chen, and P. Guyot-Sionnest, "Dual-band infrared imaging using stacked colloidal quantum dot photodiodes," *Nature Photon.*, vol. 13, no. 4, pp. 277–282, Apr. 2019, doi: 10.1038/s41566-019-0362-1.

[57] X. Tang, M. Chen, A. Kamath, M. M. Ackerman, and P. Guyot-Sionnest, "Colloidal quantum-dots/graphene/silicon dual-channel detection of visible light and short-wave infrared," *ACS Photon.*, vol. 7, no. 5, pp. 1117–1121, May 2020, doi: 10.1021/acsphotonics.0c00247.

[58] M. Ginterseder, D. Franke, C. F. Perkinson, L. Wang, E. C. Hansen, and M. G. Bawendi, "Scalable synthesis of InAs quantum dots mediated through indium redox chemistry," *J. Amer. Chem. Soc.*, vol. 142, no. 9, pp. 4088–4092, Mar. 2020, doi: 10.1021/jacs.9b12350.

[59] J. Leemans *et al.*, "Acid–base mediated ligand exchange on near-infrared absorbing, indium-based III–V colloidal quantum dots," *J. Amer. Chem. Soc.*, vol. 143, no. 11, pp. 4290–4301, Mar. 2021, doi: 10.1021/jacs.0c12871.

[60] S. Pellegrini *et al.*, "Design and performance of an InGaAs–InP single-photon avalanche diode detector," *IEEE J. Quantum Electron.*, vol. 42, no. 4, pp. 397–403, Apr. 2006, doi: 10.1109/JQE.2006.871067.

[61] J. Li, L. Wang, and S. Wei, "Electronic structure of semiconductor nanocrystals," *Pan Tao Ti Hsueh Pao, Chin. J. Semiconductors*, vol. 27, no. 2, 2006. [Online]. Available: http://www.jos.ac.cn/article/id/389c4bbf-16ba-4426-8f7a-ff3ba7c47e3d, doi: 10.1201/9781420079272-c2.

[62] Y. Yang *et al.*, "Entropic ligands for nanocrystals: From unexpected solution properties to outstanding processability," *Nano Lett.*, vol. 16, no. 4, pp. 2133–2138, Apr. 2016, doi: 10.1021/acs.nanolett.6b00730.

[63] C. Carrillo-Carrión, S. Cárdenas, B. M. Simonet, and M. Valcárcel, "Quantum dots luminescence enhancement due to illumination with UV/Vis light," *Chem. Commun.*, no. 35, p. 5214, 2009. [Online]. Available: https://pubs.rsc.org/en/content/articlelanding/2009/cc/b904381k, doi: 10.1039/b904381k.

[64] C. Xiang *et al.*, "High efficiency and stability of ink-jet printed quantum dot light emitting diodes," *Nature Commun.*, vol. 11, no. 1, Dec. 2020. [Online]. Available: https://www.nature.com/articles/s41467-020-15481-9, doi: 10.1038/s41467-020-15481-9.

[65] H. Choi, J.-G. Lee, X. D. Mai, M. C. Beard, S. S. Yoon, and S. Jeong, "Supersonically spray-coated colloidal quantum dot ink solar cells," *Sci. Rep.*, vol. 7, no. 1, Dec. 2017. [Online]. Available: https://www.nature.com/articles/s41598-017-00669-9, doi: 10.1038/s41598-017-00669-9.

Authorized licensed use limited to: Biruni Universitesi. Downloaded on November 13,2022 at 13:03:58 UTC from IEEE Xplore. Restrictions apply.